Physico-chemical Studies of the Reversible and Irreversible Phase Transitions in Potassium Ferrocyanide Trihydrate and Its Deuterate Analogue*

Masaharu OGUNI, Takasuke MATSUO, Hiroshi SUGA, and Syûzô SEKI
Department of Chemistry, Faculty of Science, Osaka University, Toyonaka, Osaka 560
(Received June 1, 1974)

Phase transitions of $K_4Fe(CN)_6 \cdot 3H_2O$ and its deuterate were studied through the measurements of differential thermal analysis curves, heat capacity, volume expansion and Raman spectra. Samples prepared by recrystallization from the aqueous solution were found to be in the metastable phase. The ferroelectric transition temperature between two stable monoclinic phases was determined to be 247.8 K and 252.7 K for the hydrate and deuterate, respectively. The enthalpy and entropy changes of the transition were estimated to be 2592 J mol^{-1} and 12.41 JK^{-1} mol^{-1}, respectively, for the hydrate, and 3017 J mol^{-1} and 14.36 JK^{-1} mol^{-1}, respectively, for the deuterate. The molecular mechanism of the transition was discussed in terms of entropy change. The transition was also concluded to be of the second order according to Ehrenfest's criterion. Irreversible transformation of tetragonal to monoclinic phase was observed for the first time for the deuterate as a new type of phase change having a Martensitic nature. These irreversible transformations took place in the temperature region covering 20 K below *ca.* 232 K and *ca.* 237 K for the hydrate and deuterate, respectively. The anhydrous salt showed no transformation in the temperature region between 13 K and room temperature.

A number of studies have been carried out on potassium ferrocyanide trihydrate and its deuterate as ferroelectrics having hydrogen-bond networks. Posperov and Zhdanov[1] (1947) disclosed the existence of both monoclinic and tetragonal crystal structures by X-ray diffraction at room temperature. Dielectric, optical and X-ray studies by Waku *et al.*,[2] Toyoda *et al.*[3] and Kiriyama *et al.*[4] also contributed to the elucidation of the structure, various types of twinning being found in particular by Toyoda *et al.* Proton and deuteron magnetic resonance methods were applied to the determination of the hydrogen position by Blinc *et al.*,[5] Tsang and O'Reilly,[6] Kiriyama *et al.*[4] and Habuda *et al.*[7] Neutron diffraction method was also applied by Taylor *et al.*[8] for the same purpose. Both the hydrate and deuterate crystals have layer structures which consist of hydrogen (or deuterium)-bonded water layers sandwiched between two double layers containing ferrocyanide octahedra and potassium ions. The monoclinic and tetragonal forms of both crystals which exist as stable and metastable modifications at room temperature, respectively, differ in the pattern of stacking of the layers, *viz.*, the layer structure can be constructed by rotating each successive layer 90° around the b-axis.[3] The monoclinic crystal has the space group C^6_{2h}–$A_{2/a}$ with four molecules in the unit cell and the tetragonal one the space group C^6_{4h}–$I_{4_1/a}$ with eight molecules in it. On being cooled, the monoclinic crystal undergoes a ferroelectric phase transition at 248.6 K and 255.1 K for the hydrate and the deuterate, respectively. The low-temperature space group is C^4_s–A_a, lacking the center of symmetry. On the other hand, the metastable tetragonal modification undergoes an irreversible phase transition to the twinned monoclinic one on being cooled below 218 K. The twinned crystal thus obtained shows only the reversible transition at 248.6 K for the hydrate on heating. The results of dielectric and optical investigations were reported for this irreversible transition by Krasnikova *et al.*[9]

The ferroelectric behavior was discovered by dielectric measurement by Waku *et al.*[10,11] in 1959. The origin of ferroelectricity can be classified into two types, the order-disorder mechanism and the displacive one. The former model involves alignment of the water molecules in the hydrogen-bonded layers, although there are two alternative models for the orientation of the water molecules as well as for the direction of spontaneous polarization.[4,6-8] Both models indicate that the compound has two different states per three water molecules at the disordered state. The latter, *viz.* the displacive mechanism, was derived from Moessbauer studies by Hazony *et al.*[12] and by Montano *et al.*[13] It involves a relative shift of the potassium ions, ferrocyanide ions and the water molecules within the crystal lattice. High pressure dielectric study was also reported by Krasnikova and Polandov[14] who constructed a phase diagram of the hydrate around the ferroelectric transition.

In spite of these studies, the thermal properties of the compound have remained relatively unexplored. The heat capacity on the monoclinic hydrate given by Nakagawa *et al.*[15] seems to be the only available datum. However, accuracy and precision of measurement were not specified and important characteristics of phase transition such as the entropy and enthalpy changes remained unclarified. We have thus investigated the properties of reversible phase transition based on the data of heat capacity and dilatometric measurements, in order to clarify the thermodynamic properties of the compounds. We have tried to elucidate the nature of the irreversible phase transition which was first discovered for the deuterate in the present investigation. The heat capacity of the anhydrous salt was also measured for the sake of comparison.

After the publication of our paper on heat capacity and dilatometric studies,[16] Malcolm *et al.*[17] reported the results of heat capacity and heat of solution on the monoclinic hydrate and anhydrous salt, and of the dissociation pressure of the monoclinic hydrate-anhydrous salt system. Compared with our results, their heat-capacity data are larger by nearly 0.5% for the hydrate except in the transition region, and smaller by about 0.6% for the anhydrous salt.

* A part of this paper has been published.[16]

Experimental

Material. The hydrate sample (special grade from Wako Pure Chemical Co., Ltd.) was recrystallized twice from its aqueous solution. The deuterate sample was prepared by recrystallization from the saturated solution in 99.75% heavy water (E. Merck) at a slow rate after dehydration of the purified hydrate *in vacuo* at 70 °C. Special care was taken to avoid photochemical decomposition. Crystals obtained were kept in a desiccator together with the anhydrous salt for over one month in order to remove excess water. The purity of the samples was determined from the weight loss caused by complete dehydration *in vacuo* at 70 °C. The water contents thus determined are given in Table 1.

Differential Thermal Analysis. Preliminary DTA studies were carried out in the transition regions for confirmation of results obtained by other workers. Details of the apparatus were already reported.[18] Granular (*ca.* 2 mm in size) and fine samples, both powdered in an agate mortar for a few minutes, were used.

Heat Capacity. The heat capacity of monoclinic modification in the range 15—300 K and that of tetragonal modification in the range 210—290 K were measured with an adiabatic calorimeter.[19] Accuracy of the measurement was better than 1% at liquid hydrogen temperature and 0.3% at room temperature. The amounts of each sample are given in Table 1. Helium gas and nitrogen gas at 100 kPa were used for the monoclinic and tetragonal samples, respectively, to facilitate heat transfer inside the calorimeter.

Monoclinic Hydrate: The sample was cooled twice down to liquid-nitrogen temperature for complete transformation to the monoclinic phase from the tetragonal modification. Samples were prepared by different methods for comparison, one being obtained by cracking a large single crystal into appropriate pieces in an agate mortar, and the other by cutting a large crystal with a razor blade. The former contained a small amount of powder in addition to the relatively large crystallites (3—5 mm), and the latter consisted of almost uniform size pieces (3—5 mm). The heat capacity curve of the crushed hydrate sample first measured showed a gentle hump in the temperature region slightly lower than the melting point of ice besides a ferroelectric phase transition. Re-examination was carried out with the same sample (see hydrate(a), Table 1) after removal of 35 mg of water from the loaded cell. The amount of water corresponds to the excess calculated from the heat-capacity hump on the assumption that it melted with the same heat of fusion as pure ice.

Monoclinic Deuterate: The same two kinds of deuterate samples as for (a) were used (see Table 1). Measurement (220—270 K) on the sample subjected to cutting treatment was carried out after the measurement of the irreversible transition region had been carried out.

Tetragonal Modification: The hydrate sample was crushed in an agate mortar, and the deuterate sample was cut with a razor blade. Measurements were carried out for samples pretreated under different pre-cooling conditions.

Dilatometric Study. The temperature dependence of the molar volume of the monoclinic hydrate was determined in the range 235—280 K in both cooling and heating with a glass-dilatometer containing degassed mercury as a confining liquid. The temperature of the methanol dry-ice bath surrounding the dilatometer was measured with a chromel-p-to-constantan thermopile. The height of the mercury column was measured with a cathetometer to the reading of 0.01 mm. The amount of the sample was determined to be 19.896 cm^3 at 26.2 °C in terms of density from X-ray data.[4]

Raman Spectroscopy. The Raman spectra of the monoclinic and tetragonal hydrates were obtained at room temperature with a Japan Spectroscopic Co., Ltd. model 750 Laser-Raman spectrometer. The incident beam was introduced parallel to the a-axis of the crystal and the scattered beam was taken out along the b-axis.

Results and Discussion

Differential Thermal Analysis (DTA). Results on the granular hydrate and deuterate recrystallized from their water and heavy water solutions, respectively, are shown in Figs. 1 and 2, respectively. In both figures Run 1 shows the cooling curves at the rate of *ca.* 1 K/min to 228 K for the hydrate and 234 K for the deuterate. These values are lower than the respective ferroelectric to paraelectric transition temperatures between their two monoclinic forms. The samples were kept for one and a half hours at the lowest respective temperatures for the purpose of testing the metastability of the tetragonal phase, and then heated up to room temperature. No change appeared throughout Runs 1 and 2, indicating that the crystals obtained were of the metastable tetragonal system, remaining metastable for a long enough time to allow calorimetric measurement in that modification. Runs 3 and 4 show the cooling curves down to 200 K and the subsequent heating ones up to room temperature, respec-

Table 1. Weights and water contents of samples

	(A)	(B)	(C)
	monoclinic modification		
hydrate(a)	61.371 g (=0.145 29 mol)	12.77%	12.794%
hydrate(b)	56.213 g (=0.133 08 mol)	12.75%	12.794%
deuterate(a)	67.302 g (=0.157 08 mol)	13.96%	14.020%
deuterate(b)	54.165 g (=0.126 42 mol)	13.97%	14.020%
	tetragonal modification		
hydrate	50.621 g (=0.119 84 mol)	12.75%	12.794%
deuterate	54.165 g (=0.126 42 mol)	13.97%	14.020%
	anhydrous salt		
	56.989 g (=0.154 71 mol)		

(A) sample weight *in vacuo*, (B) observed water content, (C) calculated water content, (a) granular crystals crushed into pieces in an agate mortar, (b) granular crystals cleaved into pieces with a razor blade.

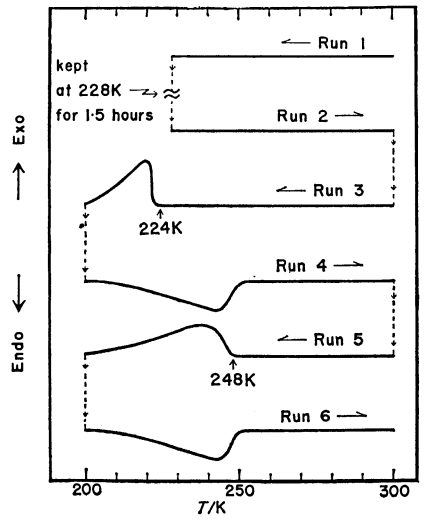

Fig. 1. DTA curves of stable and metastable $K_4Fe(CN)_6 \cdot 3H_2O$.

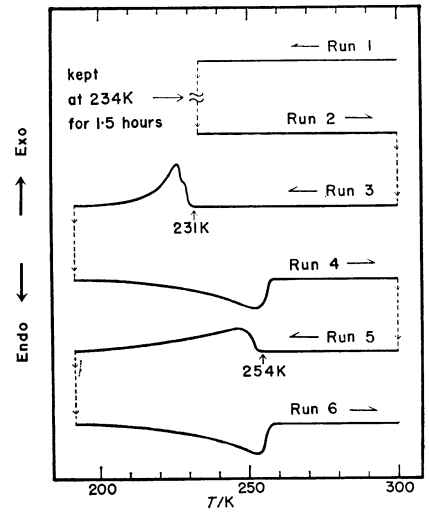

Fig. 2. DTA curves of stable and metastable $K_4Fe(CN)_6 \cdot 3D_2O$.

tively. Run 3 of the hydrate showed an exothermic effect at 234 K, whereas Run 4 no longer showed the corresponding endothermic peak but a new anomaly at 248 K. The same anomalies as found for the hydrate were observed at 231 K and 253 K for the deuterate, respectively. These results show that the metastable tetragonal crystals undergo irreversible transformation into the stable monoclinic modification when they are cooled below each transformation temperature, and that anomalies in Run 4 correspond to the reversible ferroelectric transition.

The appearance or disappearance of a shoulder in the exothermic peak in Run 3 for the deuterate changes with the sample. Runs 5 and 6 confirmed good reproducibility of the anomalies in Run 4. This indicates that the pre-cooling of the sample to a sufficiently low temperature is indispensable to studies on monoclinic modification although the sample thus obtained is heavily twinned. On the other hand, DTA curves of the powder samples did not give rise to any well-defined anomaly over the entire temperature range. The reason for this seems to be as follows. The sample might not only be partially dehydrated during the course of grinding but the surface of the crystal might also be perturbed so that complexity in the electric boundary conditions causes a broad distribution of the Curie temperatures. In fact, handling of the sample has a serious effect on experimental results, particularly with respect to the critical phenomenon.

Ferroelectric Reversible Phase Transition. Heat Capacity: The heat capacity of the crushed hydrate in the monoclinic form was measured twice. The heat capacity in the second run had no anomaly due to the loss of excess water and coincided with the first one in the temperature region below 240 K and above 273 K. A broadening at the transition point was found in the second measurement. This is attributed to partial dehydration of the sample, since the slight deficiency of water content might have a drastic effect on the shape of heat capacity curve in the transition region. Heat capacity values (13—300 K) from the first measurement (with correction for excess water) and the second measurements were adopted as the final data.

Heat capacity results are schematically shown in Fig. 3. The data of the sample obtained by cutting the crystal are adopted for respective transition regions. Selected values** for the hydrate and deuterate are given in Tables 2 and 3, respectively. Values for the sample subjected to cutting are given in series 9—11 in Table 10. Graphically smoothed heat capacities and derived thermodynamic functions for the hydrate and the deuterate are given in Tables 4 and 5, respectively. The heat capacity values of the hydrate obtained by Malcolm *et al.*[17] are larger by nearly 0.5% than the present values except in the transition region, while those obtained by Nakagawa *et al.*[15] are larger by about 50% at room temperature. We found that the anomaly due to the transition extends over a

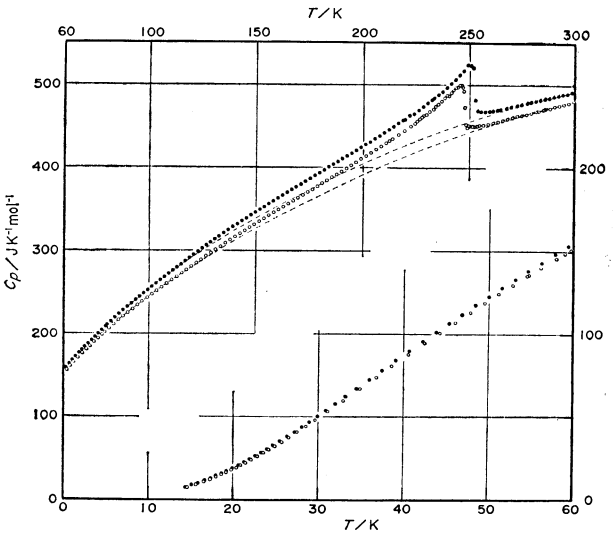

Fig. 3. Heat capacity of the monoclinic modification. ○: $K_4Fe(CN)_6 \cdot 3H_2O$, ●: $K_4Fe(CN)_6 \cdot 3D_2O$.

** The complete data of Tables 2,3,6,9 and 10 are kept as Document No. 7502 at the Chemical Society of Japan.

Table 2. Selected heat capacity data of monoclinic $K_4Fe(CN)_6 \cdot 3H_2O$

T_{av}/K	C_p/J K^{-1} mol^{-1}	T_{av}/K	C_p/J K^{-1} mol^{-1}	T_{av}/K	C_p/J K^{-1} mol^{-1}	T_{av}/K	C_p/JK^{-1} mol^{-1}	T_{av}/K	C_p/JK^{-1} mol^{-1}
		62.87	160.3	164.99	356.3	248.29	447.6	229.70	463.8
Series 1		66.54	170.4	169.52	363.3	249.58	448.0	231.87	469.4
hydrate(a)		70.55	180.5	174.01	370.5	252.17	449.0	234.00	472.8
		74.27	189.7	178.55	377.4	256.20	451.0	236.12	478.4
14.59	7.01	78.00	198.4	183.04	384.5	260.20	453.3	238.22	484.0
16.57	10.45	81.25	206.1	187.58	391.7	264.30	456.1	240.35	486.7
18.04	13.44	83.46	211.3	192.10	398.8	268.44	459.0	242.37	494.1
19.23	16.11	87.85	221.0	196.65	406.1	272.55	461.9	244.41	497.4
20.41	18.97	92.30	229.9	201.29	413.8	276.64	464.5	246.19	499.8
21.50	21.87	96.76	238.9	206.02	421.6	280.71	467.1	247.21	492.5
22.88	25.89	101.41	247.4	210.72	429.5	284.82	470.5	248.27	452.0
24.22	30.04	105.94	255.9	214.43	435.9	289.78	475.0	249.36	450.9
25.74	34.72	110.66	264.7	218.84	443.1	294.98	477.6	251.27	450.0
27.54	40.77	115.29	273.1	223.20	451.2	300.14	480.6	253.45	450.1
29.65	47.96	119.80	281.2	227.48	459.9			255.63	450.9
32.96	59.97	124.35	289.0	231.71	467.2	Series 2		261.11	454.4
36.81	74.00	128.87	297.1	235.88	476.2	hydrate(b)		265.67	457.4
40.53	87.56	133.37	304.7	239.99	483.6			270.19	460.8
44.23	100.8	137.90	312.5	243.26	490.2	205.85	421.1	274.69	463.5
47.83	113.4	142.43	320.0	244.12	491.2	210.81	429.5	279.17	466.7
51.17	124.6	146.92	327.4	245.41	491.3	216.61	439.5	285.92	471.6
54.57	135.5	151.45	334.8	246·22	492.7	222.38	449.9	290.32	474.5
56.18	140.4	155.90	342.1	246.89	488.7	255.35	455.6	294.71	477.1
59.73	151.0	160·44	349.0	247.43	480.3	227.54	460.4	299.41	481.1

Table 3. Selected heat capacity data of monoclinic $K_4Fe(CN)_6 \cdot 3D_2O$

T_{av}/K	C_p/J K^{-1} mol^{-1}	T_{av}/K	C_p/J K^{-1} mol^{-1}	T_{av}/K	C_p/J K^{-1} mol^{-1}	T_{av}/K	C_p/J K^{-1} mol^{-1}	T_{av}/K	C_p/J K^{-1} mol^{-1}
14.41	6.95	51.57	128.2	115.05	283.6	190.26	410.4	252.19	493.6
15.90	9.59	54.67	138.3	118.91	291.3	194.60	417.0	252.92	477.7
17.37	12.46	57·89	148.5	122.88	298.9	198.96	424.0	253.51	468.4
18.65	15.42	61.01	158.2	126.83	306.2	203.26	430.8	254.31	468.4
19.97	18.67	64.01	167.2	130.75	313.2	207.69	438.0	255.10	465.6
21.33	22.32	67.18	175.0	134.91	320.9	212.10	445.5	256.19	466.1
22.66	26.16	69.94	183.3	139.09	328.2	216.50	453.2	258.27	466.4
24.05	30.41	73.11	191.5	143.40	335.4	220.85	460.5	261.07	468.4
25.51	35.04	76.28	199.6	147.60	342.4	225.12	467.2	267.42	471.9
27.24	40.77	79.72	208.8	151.73	349.4	229.36	474.5	270.17	473.5
28.98	46.74	84.14	219.2	155.96	356.3	233.73	483.6	274.57	476.5
30.92	53.74	87.95	228.2	160.19	363.2	238.11	488.8	279.13	479.4
33.19	62.33	91.81	236.6	164.49	370.1	242.43	496.2	283.47	482.2
36.00	72.54	95.69	244.7	168.74	376.8	246.68	502.1	287.77	484.7
39.07	84.02	99.50	252.6	173.02	383.2	248.23	503.1	289.92	486.5
42.24	95.55	103.35	260.3	177.43	390.2	249.68	503.8	294.20	489.1
45.36	106.9	107.23	268.4	181.77	397.0	250.68	502.3	298.45	492.0
48.49	117.9	111.11	276.0	186.04	403.7	251.62	497.4	300.56	493.3

wide region of temperature, having the transition point at 247.8 K and 252.7 K*** for the hydrate and deuterate, respectively. The anomalous part was estimated by separating the normal part from the total heat capacity. The normal part, determined from the smooth extrapolation of the higher and lower temperature sides of the transition region, is thus given by the equation

$$C_p(T) = A(\ln T)^3 + B(\ln T)^2 + C(\ln T) + D + E(\ln T)^{-1} + F(\ln T)^{-2}, \quad (1)$$

where $A = -0.101196 \times 10^4$, $B = 0.240747 \times 10^5$, C=

*** The revised data of transition point, which is 0.2 K higher than the old value,[16] were taken as the more accurate temperature of the steepest drop.

Table 4. Thermodynamic functions of monoclinic $K_4Fe(CN)_6 \cdot 3H_2O$

T / K	$C_p°$ / J K^{-1} mol^{-1}	$S°-S_0°$ / J K^{-1} mol^{-1}	$[H°-H_0°]/T$ / J K^{-1} mol^{-1}	$[G°-H_0°]/T$ / J K^{-1} mol^{-1}
10	(2.25)	(0.81)	(0.60)	(0.21)
20	18.0	6.10	4.61	1.49
30	49.2	19.00	12.00	7.00
40	85.3	38.13	27.38	10.75
50	120.6	61.05	42.59	18.46
60	152.2	85.88	58.27	27.61
70	179.1	111.4	73.65	37.75
80	203.3	136.9	88.35	48.35
90	225.4	162.2	102.4	59.77
100	244.8	186.9	115.7	71.27
110	263.4	211.1	128.2	82.86
120	281.5	234.8	140.3	93.54
130	299.1	258.0	151.8	106.2
140	315.9	280.8	162.9	117.9
150	332.4	303.2	173.7	129.5
160	384.4	325.2	184.2	141.0
170	364.1	346.8	191.5	155.2
180	379.6	368.0	204.1	163.9
190	395.3	389.0	213.7	175.2
200	411.8	409.6	223.2	186.4
210	428.2	430.1	232.6	197.5
220	445.4	450.4	241.9	208.5
230	465.0	470.6	251.1	219.5
240	488.0	490.9	260.5	230.4
250	450.4	510.6	269.5	241.2
260	453.6	528.3	276.5	251.8
270	460.1	545.5	283.1	252.4
280	467.0	562.4	289.6	272.8
290	473.8	578.9	295.8	283.1
300	480.5	595.1	301.9	293.2
273.15	462.2	550.9	285.2	265.7
298.15	479.2	592.1	300.7	291.3

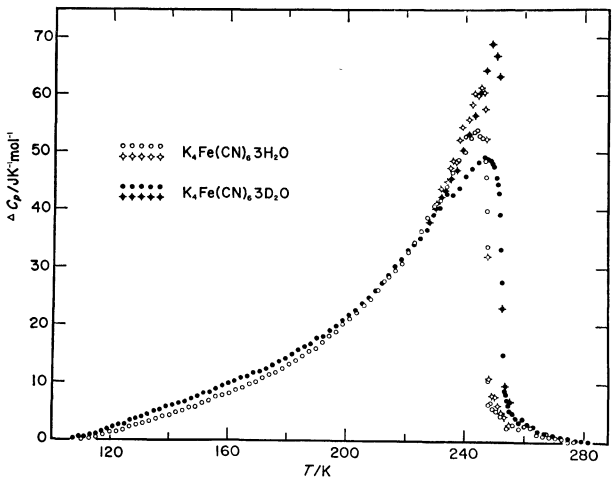

Fig. 4. Anomalous part of heat capacity of the monoclinic modification.
○ and ●: subjected to cracking treatment,
-○- and -●-: subjected to cleaving treatment.

-0.227928×10^6, $D=0.107619\times10^7$, $E=-0.253369\times10^7$ and $F=0.237844\times10^7$ for the hydrate, and $A=-0.140903\times10^4$, $B=0.340826\times10^5$, $C=-0.328633\times10^6$, $D=0.158175\times10^7$, $E=-0.379924\times10^7$ and $F=0.364163\times10^7$ for the deuterate. Figure 4 shows the anomalous part of heat capacity thus derived which does not diverge at the transition temperature. Discrepancies between the samples subjected to different treatment are of significance; the sample obtained by cutting with a razor blade has a high, sharp peak at the transition temperature as compared with that of the sample obtained by crushing into pieces. Since there is no difference in the preparation of the two samples, the discrepancy in the heat capacity is considered to be due to this difference in handling. Partial dehydration from the crystal surface and/or stacking faults including other physical impurities, both of which are possibly caused by crushing, might be responsible for the local disappearance of clearly defined critical temperature. The discrepancy between the present data and those by Malcolm *et al.* (Fig. 5) arises from a similar cause.

No anomaly was observed in the heat capacity of anhydrous salt (Fig. 6). This confirms the view that the water molecules play an essential role in the transition phenomenon. The selected data and the derived

Table 5. Thermodynamic functions of monoclinic $K_4Fe(CN)_6 \cdot 3D_2O$

T / K	$C_p°$ / J K^{-1} mol^{-1}	$[S°-S_0°]/T$ / J K^{-1} mol^{-1}	$[H°-H_0°]/T$ / J K^{-1} mol^{-1}	$-[G°-H_0°]/T$ / J K^{-1} mol^{-1}
10	(2.25)	(0.81)	(0.60)	(0.21)
20	18.6	6.210	4.705	1.51
30	50.6	19.46	14.41	5.05
40	87.5	39.05	28.06	10.99
50	122.9	62.43	43.53	18.90
60	155.1	87.68	59.48	28.20
70	183.7	113.8	75.23	38.57
80	208.9	140.0	90.36	49.62
90	232.7	160.6	104.9	61.10
100	253.7	191.6	118.7	72.90
110	273.6	216.7	131.9	84.82
120	293.4	241.4	144.5	96.89
130	311.9	265.6	156.7	108.9
140	329.6	289.4	168.4	121.0
150	346.4	312.7	179.7	133.0
160	362.8	335.6	190.7	144.9
170	378.6	358.1	201.3	156.8
180	394.4	380.2	211.6	168.6
190	409.9	402.0	221.6	180.4
200	425.4	423.4	231.4	192.0
210	442.0	444.6	241.0	203.6
220	458.5	465.5	250.5	215.0
230	476.5	486.2	260.0	226.2
240	498.2	507.0	269.4	237.6
250	524.5	527.8	279.1	248.7
260	468.7	546.8	286.9	259.9
270	474.0	564.6	293.7	270.9
280	480.0	581.9	300.3	281.6
290	486.4	598.8	306.6	292.2
300	493.0	615.4	312.7	302.7
273.15	476.0	570.1	295.8	274.3
298.15	491.7	612.4	311.6	300.8

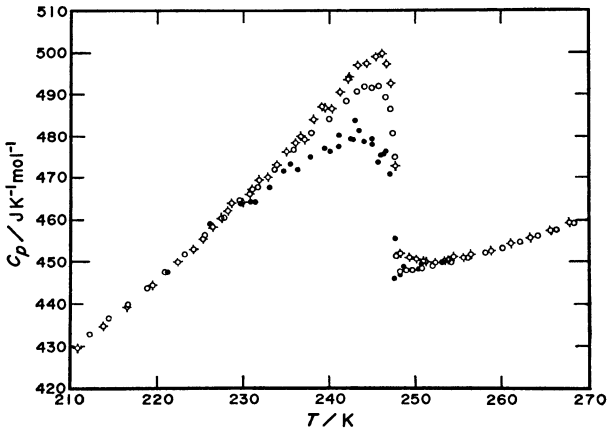

Fig. 5. Heat capacity of $K_4Fe(CN)_6 \cdot 3H_2O$ for the monoclinic modification near the transition region.
-○-: subjected to cleaving treatment,
○: subjected to cracking treatment,
●: from Ref. 17.

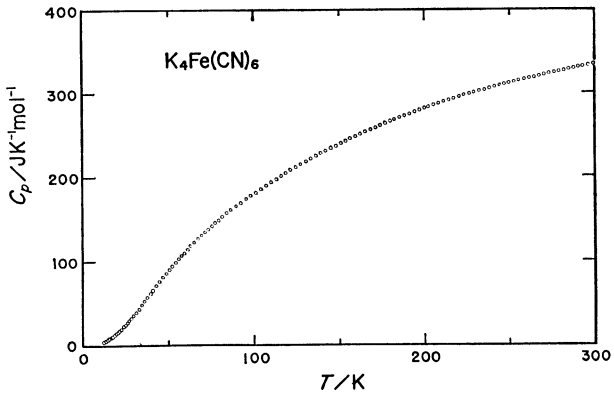

Fig. 6. Heat capacity of $K_4Fe(CN)_6$.

thermodynamic functions are given in Tables 6 and 7, respectively. The smoothed heat capacity values by Malcolm *et al.* are smaller by *ca.* 0.6% below 200 K, by *ca.* 0.8% near 250 K and by *ca.* 0.4% at 300 K than ours.

Enthalpy and Entropy Changes and the Mechanism of Phase Transition: The enthalpy and entropy changes at the transition point were estimated from the anomalous part of the heat capacities obtained. The numerical

Table 6. Selected heat capacity values of $K_4Fe(CN)_6$

T_{av}/K	C_p/J K^{-1} mol^{-1}	T_{av}/K	C_p/J K^{-1} mol^{-1}	T_{av}/K	C_p/J K^{-1} mol^{-1}	T_{av}/K	C_p/J K^{-1} mol^{-1}	T_{av}/K	C_p/J K^{-1} mol^{-1}
12.28	4.51	42.75	70.33	95.57	174.1	171.57	259.3	247.08	310.3
14.60	7.05	46.74	80.58	101.27	182.0	177.30	264.4	253.05	313.4
16.49	9.55	50.44	89.72	107.38	190.2	182.98	269.0	255.95	314.8
17.31	10.18	54.08	98.36	113.26	197.7	188.82	273.6	261.98	317.8
18.63	12.75	57.80	106.8	119.01	205.0	194.58	278.1	267.77	320.4
20.47	15.93	61.06	114.2	124.76	211.9	200.15	282.2	270.66	321.7
22.30	19.41	65.06	122.5	130.60	218.8	205.70	285.9	276.47	324.4
24.82	24.61	69.28	130.7	136.34	225.3	211.78	289.8	282.25	327.0
26.95	29.76	73.36	138.1	142.18	231.6	217.69	293.4	285.11	328.3
29.46	35.85	77.48	145.5	148.16	237.7	223.65	297.2	290.82	330.7
32.58	43.87	81.76	152.9	154.00	243.5	229.60	300.6	296.53	332.9
35.91	52.66	84.44	157.5	159.80	249.0	235.48	303.8	299.51	334.2
39.35	61.38	89.67	165.8	165.70	254.6	241.31	307.2	302.47	335.3

Table 7. Thermodynamic functions of $K_4Fe(CN)_6$

T/K	$C_p°$/J K^{-1} mol^{-1}	$[S°-S_0°]/T$/J K^{-1} mol^{-1}	$[H°-H_0°]/T$/J K^{-1} mol^{-1}	$-[G°-H_0°]/T$/J K^{-1} mol^{-1}
10	(2.19)	(0.75)	(0.58)	(0.17)
20	15.1	5.58	4.17	1.41
30	37.3	15.57	11.27	4.30
40	63.2	29.79	20.97	8.82
50	88.6	46.64	31.98	14.66
60	111.7	64.84	43.37	21.47
70	132.1	83.67	54.36	29.04
80	149.8	102.49	65.44	37.05
90	166.3	121.1	75.76	45.37
100	180.3	139.4	85.52	53.86
110	193.6	157.2	94.74	62.44
120	206.1	174.6	103.5	71.04
130	218.0	191.5	111.9	79.67
140	229.2	208.1	119.8	88.25
150	239.5	224.3	127.5	96.79
160	249.2	240.1	134.8	105.3
170	258.5	253.6	141.8	111.8
180	266.8	270.5	148.5	122.0
190	274.5	285.1	154.1	130.2
200	281.9	299.4	161.1	138.3
210	288.5	313.3	167.0	146.3
220	294.9	326.8	172.7	154.1
230	300.9	340.1	178.1	162.0
240	306.3	353.0	183.4	169.6
250	311.8	364.0	188.4	175.6
260	316.7	377.9	193.2	184.7
270	321.5	390.0	197.9	192.1
280	326.1	401.7	202.4	199.3
290	330.3	413.3	206.9	206.4
300	334.3	424.5	210.9	213.6
273.15	323.0	393.7	199.3	194.4
298.15	333.5	422.5	210.1	212.4

data are given in Table 8 together with the jump of heat capacity at the transition temperature, $\Delta C_p(T_{tr})$, where data for the sample subjected to cutting are adopted. The heat capacity jump at the transition point was estimated by the extrapolation of low and high temperature sides of C_p-values to the transition temperature by taking the rounding effect into consideration. A slight difference between the present value, 55.3 J K^{-1} mol^{-1}, and the old value,[16] 53.7 J K^{-1} mol^{-1}, for the hydrate comes from the difference in

Table 8. Thermodynamic quantities of ferroelectric reversible transition

	T_{tr} / K	ΔH_{tr} / J mol^{-1}	ΔS_{tr} / J K^{-1} mol^{-1}	ΔC_p / J K^{-1} mol^{-1}	$\Delta\alpha$ / K^{-1}
$K_4Fe(CN)_6\cdot 3H_2O$	247.8	2592 491[a)]	12.41 1.93[a)] 8.75[b)]	55.3	3.32×10^{-5}
$K_4Fe(CN)\cdot 3D_2O$	252.7	3017	14.36	68.7	

a) from Ref. 15, b) from Ref. 17.

heat capacity data; the present datum was determined from data of the cut sample and the previous one from those of the crushed sample. The entropy change of the transition thus estimated is 12.41 and 14.36 JK^{-1} mol^{-1} for the hydrate and deuterate, respectively. In the empirical classification of ferroelectric transitions, the present values of the entropy change definitely favor the order-disorder mechanism rather than the displacive one. In contrast, if we adopt the previous value 1.93 JK^{-1} mol^{-1} by Nakagawa *et al.* it may be explained also by the displacive mechanism. However, their data are not accurate enough to draw this conclusion. The entropy change expected from the structural data is $R\ln 2$ per mole of the substance, which is significantly smaller than the present values corresponding to $R\ln 4.45$ and $R\ln 5.62$ for the hydrate and deuterate, respectively.

Order of Transition: The heat capacity exhibits its jump without divergence at the transition temperature. This suggests that the transition would be of a second or higher order nature. If the phase transition is of the second order, the following Ehrenfest relation holds:

$$\left(\frac{dp}{dT}\right)_{tr} = \frac{\Delta C_p(T_{tr})}{T_{tr}V\Delta\alpha}, \tag{2}$$

where the left-hand side is the slope of the transition line, $\Delta C_p(T_{tr})$ and $\Delta\alpha$ are the jumps of heat capacity and thermal expansion coefficient, respectively, at the transition point, and T_{tr} and V the transition temperature and volume of the crystal, respectively. The volume *vs.* temperature curve for the hydrate shows no jump at the transition point. No hysteresis effect was found in the heating and cooling. This is also a characteristic of the second-order phase transitions. The best fit to the measured values is given by the following equation.

$$V_m = 0.03530\,T + 215.9170 \quad (T<248.5\text{ K}), \text{ and}$$
$$V_m = 0.02818\,T + 217.6863 \quad (T>248.5\text{ K})$$

where V_m is the molar volume in cm^3 and T in K. The change of thermal volume expansion coefficients, $\Delta\alpha$, at the transition point is 3.32×10^{-5} K^{-1}. Substitution of the measured $\Delta C_p(T_{tr})$ and $\Delta\alpha$ into the Ehrenfest relation gives 3.22×10^{7} Nm^{-2} K^{-1} for $(dp/dT)_{tr}$. This is to be compared with 3.77×10^{7} Nm^{-2} K^{-1}, the direct data of Krasnikova and others. The two values differ from each other by 17%, but the discrepancy is not significant in view of the difficulty of assessing the accuracy. The phase transition in the hydrate is of the second order or very close to it.

Energy to Reorient a Unit Dipole in the Completely Ordered State: The alignment of the water molecules is responsible for the ferroelectric transition. In the ferroelectric state, provided that the number of dipoles in the wrong orientation n is small compared with that of total dipoles N, the following approximate equation is valid;

$$\frac{n}{N} = \exp\left(\frac{\Delta s}{k}\right)\exp\left(-\frac{\Delta h}{kT}\right), \tag{3}$$

where Δh is the enthalpy required to orient a unit dipole in the environment of the almost ordered neighbors and Δs the entropy term associated with the free energy change. The anomalous heat capacity is given by

$$\Delta C_p = \frac{d(n\Delta h)}{dT} = \frac{N}{T^2}\frac{(\Delta h)^2}{k}\exp\left(\frac{\Delta s}{k}\right)\exp\left(-\frac{\Delta h}{kT}\right). \tag{4}$$

The value of $(-\Delta h/k)$ is evaluated from the slope of $\ln(\Delta C_p T^2)$ plotted against $1/T$ (Fig. 7). Linear fit to the plot between 130 and 190 K gives $n/N=13.1\times\exp(-1006/T)$ for the hydrate, and $n/N=10.4\exp(-905/T)$ for the deuterate. Thus, n/N values calculated at 190 K are 0.066 and 0.088 for the hydrate and deuterate, respectively. The reorientation enthalpies Δh are also estimated to be 8.36 and 7.52 kJ mol^{-1}, and the reorientation entropies 21.4 and 19.5 J K^{-1} mol^{-1} for the hydrate and deuterate, respectively.

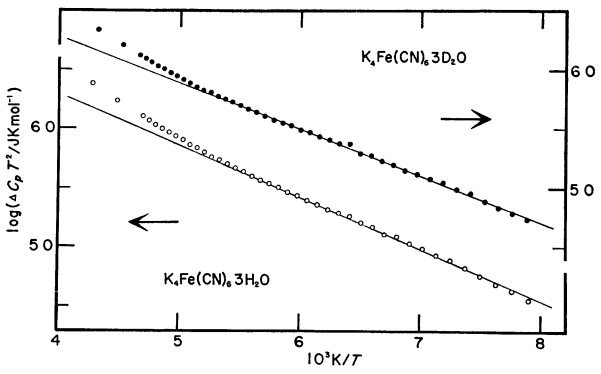

Fig. 7. Reorientation energy of a unit dipole in the completely ordered state.

The Metastable Phase and Its Irreversible Phase Transition. Heat Capacities Obtained under Different Pre-cooling Conditions: The heat capacities measured under different pre-cooling conditions are given in Tables 9 and 10 for the hydrate and deuterate, respectively. The process of measurement and results are as follows.

TABLE 9. CHRONOLOGICAL ORDER OF MEASUREMENT AND SELECTED HEAT CAPACITY VALUES FOR $K_4Fe(CN)_6 \cdot 3H_2O$ UNDER DIFFERENT PRE-COOLING CONDITIONS

room temperature —(cooling)→ 232.8 K —(measurement, 1st series)→ 288.1 K —(cooling)→ 226.0 K —(measurement, 2nd series)→ 236.1 K —(cooling)→ 229.8 K
—(measurement, 3rd series)→ 251.0 K —(cooling)→ 212.9 K —(measurement, 4th series)→ 249.6 K —(cooling)→ 221.2 K —(measurement, 5th series)→ 255.2 K —(cooling)→ 220.9 K
—(measurement, 6th series)→ 228.7 K —(cooling)→ 80 K —(heating)→ 226.4 K —(measurement, 7th series)→ 257.5 K —(cooling)→ 239.7 K —(measurement, 8th series)→ 254.5 K
—(cooling)→ 232.8 K —(measurement, 9th series)→ 257.2 —(measurement, 10th series)→ 269.0 K

T_{av}/K	C_p/J K^{-1} mol^{-1}	T_{av}/K	C_p/J K^{-1} mol^{-1}	T_{av}/K	C_p/J K^{-1} mol^{-1}	T_{av}/K	C_p/J K^{-1} mol^{-1}	T_{av}/K	C_p/J K^{-1} mol^{-1}
				245.41	472.6				
1-st series		3-rd series		246.60	460.9	7-th series		9-th series	
				250.16	446.1				
233.21	433.1	230.82	432.3			227.46	460.6	233.80	472.6
236.53	434.9	235.02	435.0	5-th series		231.50	466.9	237.66	480.5
240.93	437.5	239.19	438.1			235.48	474.6	241.58	489.5
245.52	440.3	243.34	440.3	221.81	441.5	239.41	483.8	243.52	494.2
250.14	443.6	247.46	442.1	225.93	448.0	243.27	492.0	245.45	495.4
254.73	446.8			230.56	455.0	246.75	484.5	246.91	487.2
259.29	450.1	4-th series		234.58	460.5	247.95	452.8	247.91	453.7
263.36	453.3			238.35	467.0	248.90	448.1	248.94	448.5
267.55	456.0	213.29	431.0	242.28	473.1	250.40	448.6	250.22	448.4
272.30	459.7	215.30	434.2	245.80	469.2	254.46	449.9	254.08	449.3
277.08	461.6	217.42	436.2	248.09	446.3				
282.00	466.0	219.58	439.4	251.70	447.5	8-th series		10-th series	
286.91	469.5	221.84	443.5						
		224.86	448.2	6-th series		240.63	484.1	257.80	450.9
2-nd series		229.48	455.8			242.55	487.6	259.84	452.3
		234.04	461.3	221.85	441.8	244.44	487.7	261.88	453.9
228.34	431.9	238.37	470.1	223.82	444.5	247.67	459.1	263.91	455.3
231.32	432.9	240.41	473.6	225.80	447.9	251.14	448.1	265.94	456.2
234.81	435.2	244.30	475.4	227.74	451.6	255.59	448.4	267.96	458.1

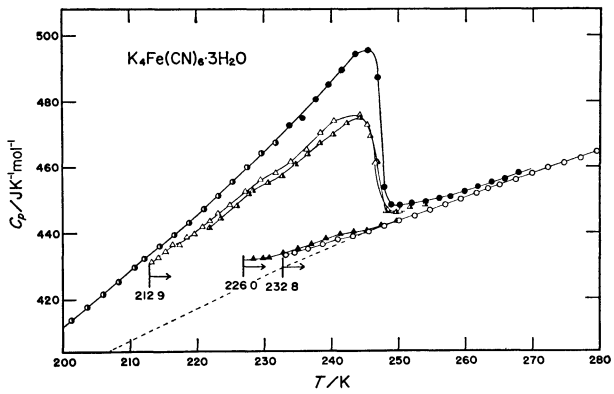

Fig. 8. Heat capacity of $K_4Fe(CN)_6 \cdot 3H_2O$ under different pre-cooling condition.
○: 1-st series, ▲: 2-nd and 3-rd series,
△: 4-th series, ◭: 5-th and 6-th series,
◑: 8-th, 9-th and 10-th series in Table 9,
●: cited from Table 2.

Measurements were carried out first in the temperature range 232.8—228.1 K with a specimen containing no monoclinic form (open circle, Fig. 8). The specimen was then cooled down to 226 K, where a slight exothermic phenomenon was observed corresponding to partial transformation of tetragonal into stable monoclinic phase. The heat capacity subsequently measured with increasing temperature (2nd and 3rd series) had a small hump in the vicinity of 240 K (symbol: ▲). This is due to the contribution of the reversible transition between the low and high temperature monoclinic phases. The 4th series (△) which started after cooling this specimen down to 212.9 K gave a much higher peak at 244 K. The measurements of the 5th and 6th (◭) series were carried out in order to confirm the reproducibility of the results under the same pre-cooling conditions. Spontaneous heat evolution was observed when the adiabatic condition was established after rapid cooling prior to measurement of the 4th series, but not of 5th and 6th series. The heat capacities of the 7th and subsequent three series coincided with those of the twinned monoclinic samples (Table 2). The heat capacity of the deuterate was measured under five different pre-cooling conditions. Reproducibility of heat capacity was checked at each stage by repeating the measurement, except for the last one in which the entire specimen was transformed into the monoclinic form. Measurement of the first series was commenced at 241.3 K

Table 10. Chronological order of measurement and selected heat capacity values for $K_4Fe(CN)_6 \cdot 3D_2O$ under different conditions

room temperature —cooling→ 241.3 K —measurement (1st series)→ 290.4 K —cooling→ 238.1 K —measurement (2nd series)→ 241.7 K —cooling→ 231.5 K —measurement (3rd series)→ 257.7 K —cooling→ 232.0 K —measurement (4th series)→ 255.4 K —cooling→ 227.3 K —measurement (5th series)→ 256.7 —cooling→ 227.8 K —measurement (6th series)→ 258.0 K —cooling→ 221.3 K —measurement (7th series)→ 256.1 K —cooling→ 222.5 K —measurement (8th series)→ 256.9 K —cooling→ 80 K —heating→ 263 K —cooling→ 232.3 K —measurement (9th series)→ 288.9 K —cooling→ 210.1 K —measurement (10th series)→ 233.2 —cooling→ 180.2 —measurement (11th series)→ 211.6 K

T_{av}/K	C_p/J K^{-1} mol^{-1}	T_{av}/K	C_p/J K^{-1} mol^{-1}	T_{av}/K	C_p/J K^{-1} mol^{-1}	T_{av}/K	C_p/J K^{-1} mol^{-1}	T_{av}/K	C_p/J K^{-1} mol^{-1}
1-st series				235.75	469.7	253.97	467.7		
		4-th series		239.78	477.8			10-th series	
				243.94	481.6	9-th series			
241.81	456.2	232.50	454.0	245.92	485.9			211.07	443.5
245.15	457.8	234.65	461.5	247.88	488.4	233.23	483.7	215.33	450.3
248.94	459.9	236.80	459.6	249.74	489.0	237.26	491.2	219.64	457.6
252.75	461.5	238.93	462.5	251.53	482.9	241.27	501.4	223.91	464.2
256.46	463.9	241.07	464.2	253.35	465.9	245.23	512.0	228.10	473.0
260.40	466.9	243.18	467.2	255.19	465.7	249.12	524.1	232.16	481.6
264.16	469.7	245.29	468.2			250.62	523.3		
268.06	472.1	246.35	469.1	8-th series		251.67	520.6	11-th series	
272.36	475.0	247.40	471.3			252.75	481.4		
276.64	478.0	248.45	472.1	223.07	459.6	255.39	467.6	181.29	395.9
280.93	480.0	249.50	473.3	226.52	464.6	259.38	468.8	183.47	400.4
285.17	482.5	250.54	473.6	230.31	471.7	263.43	471.7	185.64	402.7
287.28	484.2	251.71	469.2	234.15	478.4	267.55	472.9	187.79	406.2
289.39	486.1	252.77	464.7	238.23	484.3	271.65	475.0	189.93	409.9
				242.07	492.5	275.72	477.9	194.16	416.3
2-nd series		6-th series		246.05	501.4	279.78	480.4	198.35	423.0
				248.01	505.3	283.85	482.5	202.47	429.0
238.99	454.6	228.41	460.2	249.97	507.6	287.87	485.3	206.56	434.5
240.78	455.7	231.77	464.9	251.94	492.1	289.87	487.0	210.59	441.6

after the calorimeter had been cooled from room temperature and ended at 290.4 K. The specimen did not contain the monoclinic form at all, as evidenced by the fact that no heat capacity anomaly was observed in the 1st and 2nd series (open circle, Fig. 9). The 3rd series measured after cooling down to 231.5 K gave scattered data which coincided neither with the heat capacities of the monoclinic form nor with those of the 1st and 2nd series. The 4th series repeated under the same precooling conditions as for the 3rd one (▲) yielded a smooth curve in contrast. The heat capacity was significantly larger than that of the tetragonal form. The 5th and 6th series (◑) give heat capacities for the specimen pre-cooled to 227.3 K, which were larger than those of the previous series, the difference between heat capacities in these series being small as compared with that between the 3rd and 4th series. The difference was still less and hardly occurred between those of the 7th and 8th series (△) in which the specimen was pre-cooled to 221.3 K. The heat capacities in the 9th, 10th and 11th series (●) correspond to those of the twinned monoclinic phase. Spontaneous heat evolution was observed prior to the measurements of

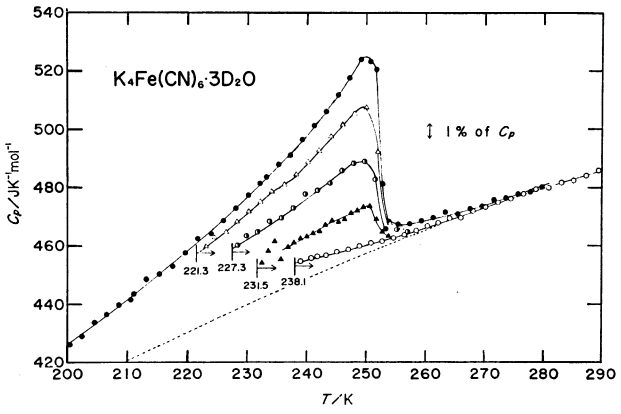

Fig. 9. Heat capacity of $K_4Fe(CN)_6 \cdot 3D_2O$ under different pre-cooling conditions.
The data of the 1-st, 2-nd (these two series: ○), 4-th (▲), 6-th (◑), 8-th (△), 9-th, 10-th and 11-th (these three series: ●) are selected by considering that these series would offer the reproducible data, while the 3-rd, 5-th and 7-th series were liable to yield scattered values.

the 3rd, 5th and 7th series as in the case of the hydrate.

From the results the following conclusions are reached. (1) The heat capacities obtained immediately after the establishment of the pre-cooling condition differ from the data of subsequent measurements performed under the same pre-cooling conditions. (2) All the data after the second agree with each other. (3) The mode of difference of heat capacity between the first and the following series depends upon the lowest temperature as well as the rate of the pre-cooling procedure, *etc.*

Similarity of the Monoclinic and Tetragonal Phases: The molecular arrangement of stable monoclinic and metastable tetragonal modifications at room temperature is quite the same in each layer and the modifications differ only in the mode of stacking. This suggests a slight difference in their lattice energies. Similarity of the two phases was also found in the Raman spectra and heat capacity values. The Raman spectra of each phase at room temperature were found to be in complete agreement except for a slight difference in intensity. Good coincidence in heat capacity and its dependence is shown in the case of the deuterate in Fig. 9. For the hydrate this cannot be definitely concluded for lack of data on the same sample in the temperature range where the short range ordering of the water molecules in the monoclinic phase is expected to vanish. However, between these two phases a distinct similarity in the thermal motion, and also in total enthalpy and entropy at room temperature is expected.

Properties of the Metastable Tetragonal Phase: The hydrate crystal in the tetragonal modification does not transform into the monoclinic phase in the temperature range between 232.8 K and room temperature. The tetragonal modification for the deuterate remains metastable at temperatures above 238 K. This is evident from the absence of heat capacity anomaly which should appear in the monoclinic modification (open circle, Figs. 8 and 9). It should be added that the hydrate sample crystals could be kept in a desiccator for six months without transformation. The heat capacity curve of the tetragonal modification (Figs. 8 and 9) deviates anomalously around 240 K. This is also the case for the tetragonal deuterate. The anomalous shape of the heat capacity curve suggests further contribution of a configurational one due to the development of the short range order of water molecule. In view of the structural similarity of the monoclinic and tetragonal phases within the hydrogen-bonded layer, the water molecules would be ordered in each layer around the same temperature where the stable monoclinic-monoclinic transition takes place.

Nature of the Phase Transition: The irreversible exothermic transformation of the tetragonal phase into the *twinned* monoclinic phase takes place below 232 K for the hydrate and below 237 K for the deuterate. This phase transformation develops in a strange way and is to some extent characteristic of the lowest temperature to which the specimen has been chilled down. Thus, the heat capacity curves measured exhibit different behaviors in accordance with the pre-cooled lowest temperatures (Tables 9 and 10, Figs. 8 and 9). In the

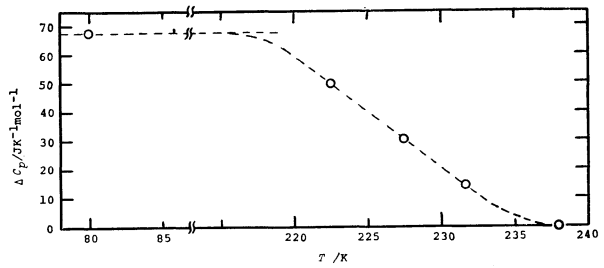

Fig. 10. The dependence of the peak heights of heat capacity on pre-cooling temperatures in $K_4Fe(CN)_6 \cdot 3D_2O$.

case of the deuterate the heat capacity peaks for the samples pretreated under different pre-cooling conditions appear at *the same temperature* 250 K, at which the pure monoclinic-monoclinic phase transition takes place. This indicates that the original tetragonal and the partially grown monoclinic phases coexist independently so that the peak height of the heat capacity has a linear relation to the ratio of amounts of the monoclinic to the tetragonal phases. The relation between the peak height and the precooled temperature is given in Fig. 10. This peculiar behavior suggests that the metastability of the tetragonal phase is due not to the absence of the nucleation by which the tetragonal phase is transformed into the complete monoclinic phase, but to the nature of the transformation: *viz.* in spite of enough macroscopic amount of stable monoclinic phase, the transformation in this crystal stops at any intermediate stage. This was evidenced by cessation of spontaneous heat evolution and also by the reproducibility of heat capacity data as long as the sample was not cooled below the lowest temperature to which the specimen had been brought. This new type of phase transformation with the characteristics of the Martensitic one[20] rarely observed in non-metals might occur from the following viewpoint based on the free energy difference between the monoclinic and tetragonal phases. The transformation does not seem to occur until the driving force attains a characteristic threshold value as in the case of Martensitic transition. This driving force will be given by the free energy difference between the two phases. On the other hand, the threshold value may arise from the sum of the interface and/or strain free energies, *etc.* associated with the creation of *twinned* monoclinic phase and it becomes larger with the increased amount of this monoclinic phase. As long as there is no reversible transformation in the tetragonal phase, the free energy diagram is such as depicted schematically in Fig. 11 for the deuterate, where the dotted area stands for the transformation region experimentally confirmed. The free energy difference at room temperature is imagined to be fairly small from similarity in structure as well as in thermal motion between the two modifications. This difference will increase with a fall in temperature through the reversible ferroelectric transition, since the heat capacity is larger for the monoclinic form than that for the tetragonal. The actual transformation will be initiated when the threshold value is reached with

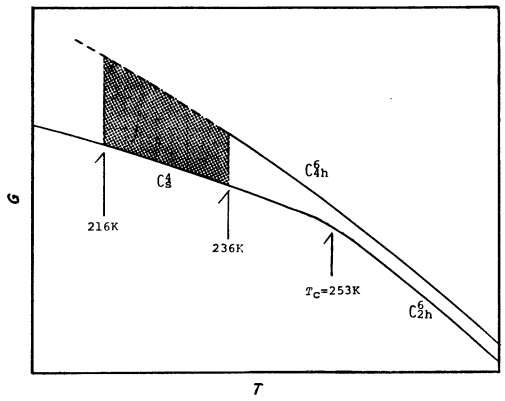

Fig. 11. Schematical free energy diagram of $K_4Fe(CN)_6 \cdot 3D_2O$. The upper curve, C_{4h}^6, corresponds to the tetragonal modification. The portion, C_{2h}^6, of the lower curve stands for the paraelectric monoclinic phase, and the portion, C_s^4, for the ferroelectric monoclinic phase. Dotted area is of the irreversible transition region to the monoclinic form.

decreasing temperature. If production of the *twinned* monoclinic phase were to lead to an increase of the threshold value preventing further transformation, the process would be stopped at the intermediate stage which is constrained by the balance between the temperature dependent-free-energy difference of two phases and the threshold value determined by the amount of the coexisting monoclinic phase. This view will also explain why the difference between the Curie temperature and the irreversible transition temperature is almost the same for the hydrate and deuterate, since the anomalous heat capacities behave analogously for these two compounds.

The created monoclinic crystal in the tetragonal phase has a *twinned* structure. In parallel with this it is interesting that the Martensitic materials are often composed of an assembly of thin plates.

According to the report of Krasnikova *et al.* in which irreversible transition was studied through the measurement of double refraction, the irreversible transition temperature becomes higher with the increase in the monoclinic fraction of a macroscopic sample. Our results indicate the opposite tendency as regards the transition point. This apparent contradiction will necessitate further elucidation of the intrinsic properties or textures of starting materials they used.

The Rate of Phase Transformation: A spontaneous temperature rise accompanied with irreversible transformation was observed immediately after rapid precooling. This phenomenon was carefully followed at five different temperatures in the transition region for the deuterate, an example being in Fig. 12. The procedure taken for every measurement of the spontaneous temperature rise was always the same. After the calorimeter was first cooled to a temperature 2 K above that at which the measurement was started, adiabatic conditions were established, and then the calorimeter was cooled again by introducing the exchange gas into the cryostat. When the desired temperature was reached, the cryostat was evacuated and the adiabatic control system was started to function. This round-about pro-

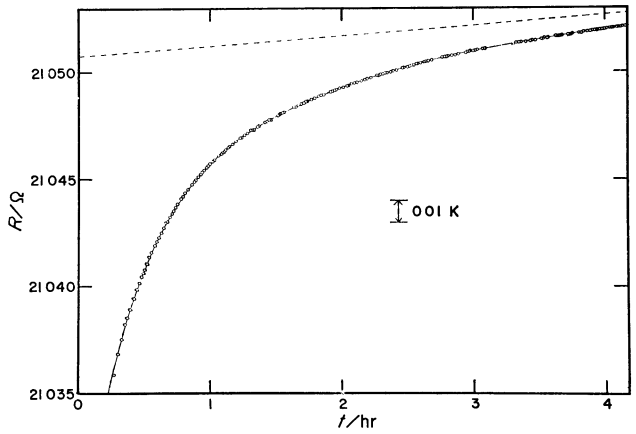

Fig. 12. A spontaneous heat evolution after rapid pre-cooling.

cedure was designed to realize as similar a cooling rate and temperature distribution in the cryostat as possible for each measurement. A control run performed after the entire specimen was transformed into the monoclinic form showed that the heat leak effect was small enough to be neglected as compared with the observed temperature rise. The broken line in Fig. 12 shows the natural drift observed in the control run. We tried to fit the time dependence of temperature into an exponential law with single time constant τ, on the assumption that the molar enthalpies of the monoclinic and tetragonal phases and the heat capacity of the calorimeter cell containing the sample were constant during the course of measurement. The time constant was evaluated with an estimated error of 20%, the observed temperature rise being fitted to the following equation.

$$T(t) - T(\infty) = A \exp(-t/\tau), \qquad (5)$$

where T and t are temperature and time, respectively, and A is a numerical constant. Fig. 13 shows the temperature dependence of the time constant which corresponds to the half-life. The value of τ decreases with decreasing temperature, except at the lowest

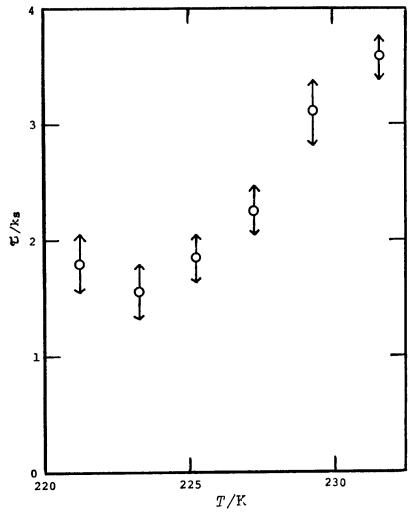

Fig. 13. Temperature dependence of time constant of spontaneous heat evolution in $K_4Fe(CN)_6 \cdot 3D_2O$.

temperature, in contrast to a thermal activation process. Explanation should be given taking into account the free energy difference between the tetragonal and monoclinic phases as the driving force of the transformation. The simplest expression will be

$$\frac{dX_m}{dt} = -B\{X_m(t)-X_m(\infty)\}\Delta G \qquad (6)$$

where X_m, B and ΔG stand for the molar fraction of the monoclinic phase, some positive constant dependent on temperature, and the free energy difference between the two phases, respectively. The time constant in Eq. (5) is identified with $1/(B\Delta G)$. As ΔG increases with decreasing temperature (Fig. 11), the initial decrease of τ on cooling can be attributed to the increase in the driving force of the transformation. The increase in the time constant by further decreasing temperature can be ascribed to the temperature factor through constant B.

Conclusion

Thermal properties we obtained give important information on the stability and phase transitions of $K_4Fe(CN)_6 \cdot 3H_2O$ and its deuterate. The amount of entropy change at the ferroelectric transition between two stable monoclinic phases strongly suggests the molecular mechanism of an order-disorder type. Behavior of heat capacity and molar volume changes at the transition point indicates that this phase change is very close to the second-order type, the Ehrenfest relation for the second-order phase transitions being found to hold. This is a rare example of the second-order transition tested by Ehrenfest's relation.

The metastable tetragonal crystals underwent an irreversible transition to the stable monoclinic phase. The transition was found to be a new type with some characteristics of the Martensitic transition which is rarely found in non-metallic compounds.

We wish to thank Professors Ryoichi Kiriyama and Hideko Kiriyama for fruitful discussions. We are grateful to Mr. Mitsuo Ôhama for the measurements of Raman spectra.

References

1) V. A. Pospelov and G. S. Zhdanov, *Zh. Fiz. Khim. SSSR*, **21**, 405, 521, 879 (1947).
2) S. Waku, K. Masuno, T. Tanaka, and H. Iwasaki, *J. Phys. Soc. Japan*, **15**, 1185 (1960).
3) H. Toyoda, N. Niizeki, and S. Waku, *J. Phys. Soc. Japan*, **15**, 1831 (1960).
4) R. Kiriyama, H. Kiriyama, T. Wada, N. Niizeki, and H. Hirabayashi, *ibid.*, **19**, 540 (1964).
5) R. Blinc, M. Brenman, and J. S. Waugh, *J. Chem. Phys.*, **35**, 1770 (1961).
6) T. Tsang and D. E. O'Reilly, *ibid.*, **43**, 4234 (1955).
7) S. P. Habuda, A. G. Lundin, and E. P. Zeer, *Ferroelectrics*, **1**, 71 (1970).
8) J. C. Taylor, M. H. Mueller, and R. H. Hitterman, *Acta Crystallogr*, **A26**, 559 (1970).
9) A. Ya. Krasnikova, V. A. Koptsik, B. A. Strukov, and Wang Ming, *Sov. Phys. Solid State*, **9**, 85 (1967).
10) S. Waku, H. Hirabayashi, H. Iwasaki, and R. Kiriyama, *J. Phys. Soc. Japan*, **14**, 973 (1959).
11) S. Waku, K. Masuno, and Y. Tanaka, *ibid.*, **15**, 1698 (1959).
12) Y. Hazony, D. E. Earls, and I. Lefkowitz, *Phys. Rev.*, **166**, 507 (1968).
13) P. A. Montano, H. Shecter, and U. Shimony, *ibid.*, **B3**, 858 (1971).
14) A. Ya. Krasnikova and I. N. Polandov, *Sov. Phys. Solid State*, **11**, 1421 (1970).
15) T. Nakagawa, S. Sawada, T. Kawakubo, and S. Nomura, *J. Phys. Soc. Japan*, **18**, 1227 (1963).
16) T. Matsuo, M. Oguni, H. Suga, and S. Seki, *Proc. Japan Acad.*, **48**, 237 (1972).
17) I. R. Malcolm, L. A. K. Staveley, and R. D. Worswick, *Trans. Faraday Soc.*, **A69**, 1532 (1973).
18) H. Suga, H. Chihara, and S. Seki, *Nippon Kagaku Zasshi* **82**, 24 (1961).
19) H. Suga and S. Seki, This Bulletin, **38**, 1000 (1965).
20) L. Kaufman and M. Cohen, *Prog. Met. Phys.*, *Pergamon Press*, **7**, 165.